MNRAS 000, 1–6 (2019) Preprint 18 July 2019 Compiled using MNRAS LaTeX style file v3.0

Cassini State Capture

Yubo Su[1], Dong Lai[1]
[1] *Cornell Center for Astrophysics and Planetary Science, Department of Astronomy, Cornell University, Ithaca, NY 14853, USA*

Accepted XXX. Received YYY; in original form ZZZ

ABSTRACT
Abstract

Key words: planet–star interactions

1 INTRODUCTION

Introduction, test citation (Henrard 1982).

2 CASSINI STATES

Denote $\hat{s}$ spin of planet, $\hat{l}$ angular momentum of planet, and $\hat{l}_p$ angular momentum of perturber. The Cassini state Hamiltonian in the frame corotating with $\hat{l}_p$ about $\hat{l}$ is:

$$H = -\frac{\alpha}{2}\left(\hat{s}\cdot\hat{l}\right)^2 - g\left(\hat{s}\cdot\hat{l}_p\right). \tag{1}$$

$\alpha > 0, g < 0$ depend on the particular dynamics of the system. Frequently, parameter

$$\eta \equiv \frac{|g|}{\alpha} \tag{2}$$

is defined; we refrain from doing so immediately.

Choose $\hat{l} = \hat{z}$ and $\hat{l}_p = \cos I\hat{z} + \sin I\hat{x}$. Furthermore, choose standard convention where $\phi = 0$ corresponds to $\hat{l}_p, \hat{s}$ lying on *opposite* sides of $\hat{l}$. This allows us to evaluate Hamiltonian

$$H = -\frac{\alpha}{2}\cos^2\theta + |g|\left(\cos\theta\cos I - \sin I\sin\theta\cos\phi\right) \tag{3}$$

Here, $\mu \equiv \cos\theta, \phi$ are canonically conjugate.

2.1 Equilibria

The evolution of $\hat{s}$ in this corotating frame is governed by:

$$\frac{\mathrm{d}\hat{s}}{\mathrm{d}t} = \alpha\left(\hat{s}\cdot\hat{l}\right)\left(\hat{s}\times\hat{l}\right) - |g|\left(\hat{s}\times\hat{l}_p\right). \tag{4}$$

Spin states satisfying $\frac{\mathrm{d}\hat{s}}{\mathrm{d}t} = 0$ are referred to as *Cassini States* (CS). When $\eta < \eta_c$, there are four CSs, and when $\eta > \eta_c$ there are only two; η_c is

$$\eta_c \equiv \left(\sin^{2/3} I + \cos^{2/3} I\right)^{3/2}. \tag{5}$$

Using the standard numbering given in Figure 1, CSs 1, 2, 3 are stable while CS4 is unstable.

2.2 Separatrix

In the four-CS regime, one of the CSs is a saddle point, conventionally denoted Cassini State 4 (CS4). On the cylindrical phase space parameterized by (μ, ϕ), all trajectories are periodic with finite period except two critical (or heteroclinic) trajectories. These are asymptotic in the past and future to CS4. Together, these two heteroclinic are referred to as the *separatrix* and divide phase space into three zones.

The area enclosed by the separatrix is known exactly in literature (Henrard & Murigande 1987), but a serviceable approximation for small η can be derived as follows. Call H_4 the value of H at CS4, then the separatrix is defined implicitly by solutions to $H\left(\mu_{sep}(\phi), \phi\right) = H_4$. This may be evaluated and we obtain

$$\mu_{sep}(\phi) \approx \pm\sqrt{2\eta\sin I\left(1-\cos\phi\right)} + \eta\cos I + O\left(\eta^{3/2}\right). \tag{6}$$

The enclosed area between the two solutions can be obtained via explicit integration. It can be expressed as a fraction of the total phase space area:

$$\frac{A_{sep}}{4\pi} \approx \frac{4\sqrt{\eta\sin I}}{\pi} + O\left(\eta^{3/2}\right). \tag{7}$$

Contours of equal H, CSs and the separatrix are plotted in Figure 1.

3 SEPARATRIX CROSSING: THEORY

In an exactly Hamiltonian system, H is a conserved quantity and trajectories in phase space coincide with level curves of H. If a system is only slightly non-Hamiltonian, trajectories will generally cross level curves. Of particular interest is the behavior of trajectories near the separatrix (also a level curve), as it frequently governs the dynamics of resonance capture (CITE MMR, Cassini, others). The intersection of system trajectories with the separatrix is referred to as *separatrix crossing*.

In previous work by Henrard (1982), separatrix crossing was studied for systems that are Hamiltonian save for an adiabatically-varying parameter. In related work surveyed by Guckenheimer & Holmes (1983), the impact of small perturbations to the equations of motion of a Hamiltonian system are studied (referred to as *saddle connection bifurcations*). However, in some astrophysical systems

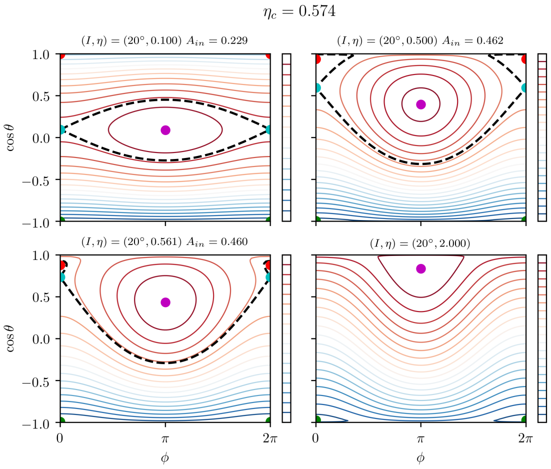

Figure 1. Contours of equal H, given by Equation 3, at different values of $\eta \equiv \frac{|g|}{\alpha}$. Labeled are CS1 (red), CS2 (purple), CS3 (green) and CS4 (cyan). The thick black dashed line is the separatrix (which disappears for $\eta > \eta_c$). Finally, the fractional area enclosed by the separatrix is noted in the plot subtitles, in good agreement with Equation 7.

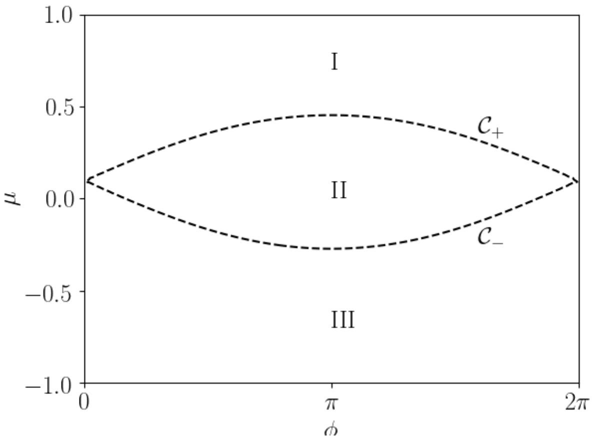

Figure 2. Nomenclature of the two legs of the separatrix $C_\pm$ and three zones of the domain. For both $C_\pm$, we will take the positive direction to be anti-clockwise.

of interest, leading-order perturbations to a Hamiltonian system contribute in both of the above ways. Such systems resist characterization via either existing technique. We suggest a possible generalization unifying the above techniques. [Probably eventually move this paragraph to the introduction]

3.1 Derivation

Consider our Hamiltonian described in Equation 3 as a unperturbed Hamiltonian $H^{(0)}(\mu, \phi; \eta)$ where η is to be varied adiabatically. As η varies, the location of the separatrix also changes. We follow Henrard (1982) by defining

$$h(\mu, \phi; \eta) \equiv H^{(0)}(\mu, \phi; \eta) - H_4(\eta). \tag{8}$$

The significance of h is that it always vanishes along the separatrix. Note that h corresponds to K in Henrard (1982), though in our problem $H^{(0)} > H_4$ corresponds to the *interior* of the separatrix. The evolution of h over time then determines whether and when a trajectory experiences separatrix crossing. Denoting time derivatives with dots, we write

$$\begin{aligned}
\frac{\mathrm{d}h}{\mathrm{d}t} &= \frac{\mathrm{d}H^{(0)}}{\mathrm{d}t} - \frac{\partial H_4}{\partial \eta}\dot{\eta},\\
&= \left[\frac{\partial H^{(0)}}{\partial \mu}\dot{\mu} + \frac{\partial H^{(0)}}{\partial \phi}\dot{\phi} + \frac{\partial H^{(0)}}{\partial \eta}\dot{\eta}\right] - \frac{\partial H_4}{\partial \eta}\dot{\eta},\\
&= \left[\frac{\partial H^{(0)}}{\partial \mu}\dot{\mu} + \frac{\partial H^{(0)}}{\partial \phi}\dot{\phi} + \frac{\partial H^{(0)}}{\partial \eta}\dot{\eta}\right] - \frac{\partial H_4}{\partial \eta}\dot{\eta},\\
&= \left[\dot{\phi}^{(0)}\dot{\mu}^{(1)} - \dot{\mu}^{(0)}\dot{\phi}^{(1)} + \frac{\partial H^{(0)}}{\partial \eta}\dot{\eta}\right] - \frac{\partial H_4}{\partial \eta}\dot{\eta}.
\end{aligned} \tag{9}$$

We've notated $\dot{\phi}^{(0)} \equiv \frac{\partial H^{(0)}}{\partial \mu}$ and $\dot{\phi}^{(1)} = \dot{\phi} - \dot{\phi}^{(0)}$ and similarly for μ. The scenario studied in Henrard (1982) corresponds to $\dot{\mu}^{(1)} = \dot{\phi}^{(1)} = 0$ while that in Guckenheimer & Holmes (1983) sets $\dot{\eta} = 0$.

In the neighborhood of $C_\pm$, $\frac{\mathrm{d}h}{\mathrm{d}t}$ can be approximated by its value on $C_\pm$. This is the *guiding orbit* approximation; its accuracy is proven in Henrard (1982) for their specific application, while we will take it on good faith in ours. Denote then

$$\Delta_\pm \equiv \int_{C_\pm} \frac{\mathrm{d}h}{\mathrm{d}t}\,\mathrm{d}t. \tag{10}$$

These approximate Δh for trajectories near $C_\pm$ over one orbit. They are identical to the B_i defined in Henrard (1982).

For concreteness, we consider a specific example first. We assign labels to our phase space as shown in Figure 2. Consider a trajectory that begins in zone III, which is circulating with $\dot{\phi} > 0$ and has $h < 0$, and consider if $\frac{\mathrm{d}h}{\mathrm{d}t} > 0$ in all of zone III, such that the trajectory eventually experiences separatrix crossing at C_-. The following sequence of events unfolds:

(i) At the beginning ($\phi = 0$) of its separatrix-crossing orbit, $h_i \equiv h(\mu, \phi = 0; \eta) \in (\Delta_-, 0)$. Note that $h_i < 0$ to still be in zone III at the start of the orbit, while $h_i > \Delta_-$ to be separatrix crossing during the final orbit.

(ii) After traversing the length of C_-, the value of h is now $h_i + \Delta_- > 0$ (recall $\Delta_- > 0$), and so the trajectory has entered zone II. Since zone II hosts only librating solutions, the trajectory will then "turn around" and track C_+ from inside zone II.

(iii) At the end of following C_+, h now takes value $h_f \equiv h_i + \Delta_- + \Delta_+$. There are now two possibilities:

(iii-a) If $h_f > 0$, the trajectory remains inside zone II accrues further multiples of $\Delta_- + \Delta_+ = h_f - h_i > 0$. Thus, the trajectory must securely enter zone II. This outcome commonly corresponds to *resonance capture*, a transition into zone II.

(iii-b) If $h_f < 0$, the trajectory exits zone II and enters zone I. Since $\Delta_+ = h_f - h_i - \Delta_- < 0$ (as $h_f < 0, h_i + \Delta_- > 0$), the trajectory will continue circulation in zone I and accrue further multiples of Δ_+, securely entering zone I. This corresponds to a zone III-zone I transition, *escape*.

Thus, the result of separatrix crossing depends on the sign of $h_i + \Delta_- + \Delta_+$ where $\Delta_\pm$ are given by Equation 10 and $h_i \in [-\Delta_-, 0]$. The result of this analysis reproduces the conclusion of Henrard (1982):

- If $\Delta_+ < -\Delta_-$, then $h_f < 0$ necessarily, secure escape ensues.
- If $\Delta_+ > 0$, then $h_f > 0$ necessarily, and secure capture ensues.
- If $\Delta_+ + \Delta_- \in [0, \Delta_-]$, then it is clear that the sign of h_f depends on the precise value of h_i. Generally, Δ_- can be assumed

to be small as perturbations are weak, and so Δ_- is usually much smaller than the range of h of interest. Thus, h_i can be treated as uniformly distributed on interval $[-\Delta_-, 0]$, and a probability of resonance capture can be computed:

$$P_c \equiv \frac{\Delta_+ + \Delta_-}{\Delta_-}. \tag{11}$$

With the exception of Equation 9, the above outlines the argument given in Henrard (1982).

Similar derivations can be given for trajectories originating in zone I. TODO say something about zone-II originating systems.

3.2 Equivalence to Stable/Unstable Manifold Splitting

We now establish equivalence to an alternative formulation popular in dynamical systems that is more graphically intuitive. For simplicity, we will take $\dot{\eta} = 0$.

If we return to the unperturbed Hamiltonian system, recall that CS4 is joined to itself by an infinite-period orbit. For a given saddle point, we may define the *stable manifold* W_s of a saddle point to be the set of points whose forward evolution converges to the saddle point. Similarly, we may define the *unstable manifold* W_u of a saddle point to be the set of points that originated *from* the saddle point, or whose backwards evolution converges to the saddle point. A *saddle connection* is when the unstable manifold of one saddle point and the unstable manifold of another saddle point are degenerate. It is evident that the separatrix is formed of two saddle connections: C_+ is the unstable manifold of CS4 at $\phi = 2\pi$ and the stable manifold of CS4 at $\phi = 0$.

In the presence of a small perturbation, the stable and unstable manifolds generally separate, as the perturbations along the saddle connection will generally be different going forwards and backwards in time. The separation distance as a function of time along the *unperturbed* trajectory can be computed via *Melnikov's Method*

$$d(t_0) = \frac{\epsilon}{\left|f(q^0(-t_0))\right|}\int_{-\infty}^{\infty} f(q^0(t - t_0)) \wedge g(q^0(t - t_0), t)\,\mathrm{d}t. \tag{12}$$

The notation used here is that of Guckenheimer & Holmes (1983), where $d(t_0)$ is the distance between the stable/unstable manifolds at time t_0 along the heteroclinic orbit, $f = \left(\dot{\mu}^{(0)}, \dot{\phi}^{(0)}\right)$, $\epsilon g = \left(\dot{\mu}^{(1)}, \dot{\phi}^{(1)}\right)$ a general time-dependent perturbation, $q^0(t)$ is the unperturbed trajectory along the saddle connection (time coordinate defined such that $t = 0$ coincides with the "middle" of the infinite trajectory), and $\wedge$ is the wedge product.

We will assume ϵg is not explicitly time-dependent, characteristic of secular/averaged equations in astrophysics, then the integral above is simply the familiar

$$d(t_0)\left|\vec{\nabla} H^{(0)}\right|(t_0) = \epsilon\int_{-\infty}^{\infty} \dot{\mu}^{(0)}\dot{\phi}^{(1)} - \dot{\phi}^{(0)}\dot{\mu}^{(1)}\,\mathrm{d}t. \tag{13}$$

The right hand side is just the total change in $H^{(0)}$ over the saddle connection though, equivalent to our Equation 10 in the $\dot{\eta} = 0$ limit. The left hand side on the other hand is exactly $\left|\vec{d}\cdot\vec{\nabla} H^{(0)}\right|$ where the displacement is along $\vec{\nabla} H^{(0)}$. Thus, the effect of the $\Delta_\pm$ is to split the stable/unstable manifolds along the saddle connections.

Visually, this is depicted in Figure 3. Note that: trajectories starting in zone III below $W_s^{(1)}$ fail to separatrix cross; those between $W_s^{(1)}$ and $W_s^{(0)}$ continue between $W_u^{(1)}$ and $W_s^{(0)}$, eventually escaping; those between $W_s^{(0)}$ and $W_u^{(0)}$ are securely captured, and no trajectories can begin above $W_u^{(0)}$ at $\phi = 0$.

The saddle connection splitting is easiest to measure where $\vec{\nabla} H^{(0)} \propto \hat{\phi}$, where $\dot{\mu} = 0$, and Equation 13 reduces to just $\Delta\mu\frac{\partial H^{(0)}}{\partial\mu} = \Delta H^{(0)}$. Then the capture probability must be given by ratio of $\Delta\mu$ separating $W_s^{(0)}, W_u^{(0)}$ to $\Delta\mu$ separating $W_s^{(1)}, W_u^{(0)}$. These $\Delta\mu$ values are those given in the title, and the resultant P_c capture probability is also quoted.

Finally, the connection between subsection 3.1 and subsection 3.2 is evident: the ratio of the $\Delta\mu$ values is simply

$$P_c = \frac{\Delta\mu(W_s^{(0)}, W_u^{(0)})}{\Delta\mu\left(W_s^{(1)}, W_u^{(0)}\right)},, \tag{14}$$

$$= \frac{\Delta H_-^{(0)} + \Delta H_+^{(0)}}{\Delta H_-^{(0)}}. \tag{15}$$

This is exactly Equation 11 when $\dot{\eta} = 0$.

[t]

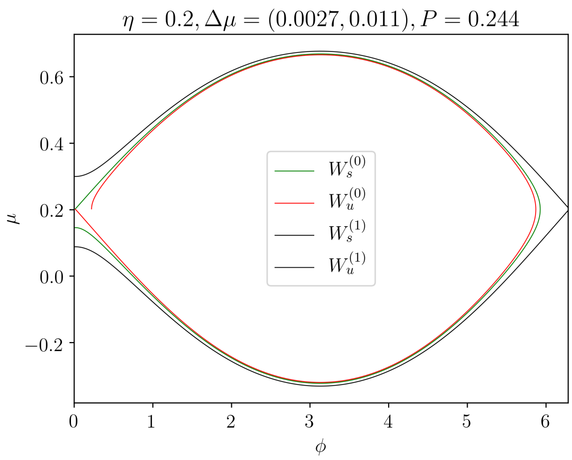

Figure 3. Sample plot of saddle connection breaking in the presence of weakly non-Hamiltonian dissipation. Equations are used from Section 4. Stable and unstable manifolds are indexed such that superscript (0)/(1) belongs to the saddle point at left/right. $\Delta\mu$ represent the manifold separations, resulting in capture probability P_c prediction per Equation 14. Numerical simulations predict $P_c \approx 0.252$.

4 PROBLEM 1: WEAKLY DISSIPITIVE HAMILTONIAN

We first consider a toy separatrix crossing problem in the $\dot{\eta} = 0$ limit, the case discussed in subsection 3.2. Consider adding to the Hamiltonian Cassini State problem an additional aligning term $\left(\frac{\mathrm{d}\theta}{\mathrm{d}t}\right)^{(1)} = -\frac{1}{t_s}\sin\theta$ that favors alignment $\theta = 0$ on synchronization timescale t_s. This translates to equation of motion

$$\frac{\mathrm{d}\hat{s}}{\mathrm{d}\tau} = \left(\hat{s}\cdot\hat{l}\right)\left(\hat{s}\times\hat{l}\right) - \eta\left(\hat{s}\times\hat{l}_p\right) - \epsilon\sin\theta\hat{\theta}. \tag{16}$$

We have divided Equation 4 by α and defined $\tau \equiv \alpha t, \epsilon \equiv \frac{1}{\alpha t_s}$. The equations of motion for canonical variables $\mu \equiv \cos\theta, \phi$ are

$$\mu' = -\cos\theta + \eta\left(\cos I + \sin I\frac{\mu}{\sqrt{1-\mu^2}}\cos\phi\right), \tag{17a}$$

$$\mu' = -\eta\sin I\sin\theta\sin\phi\left[+\epsilon\left(1-\mu^2\right)\right]. \tag{17b}$$

Primes denote $\frac{\mathrm{d}}{\mathrm{d}\tau}$. The bracketed term in μ' is the perturbation component.

With a dissipitive term that favors alignment, we expect that separatrix encounters can only occur from zone II and zone III. We will focus on the outcomes of trajectories origiating in zone III for now. We now aim to compute Equation 11, for which we need:

$$\Delta_- = \int_{C_-} \phi' \epsilon \left(1 - \mu^2\right)\,\mathrm{d}t, \\ = \int_{C_s} \left(1 - \mu^2\right)\,\mathrm{d}\phi, \tag{18a}$$

$$\Delta_- + \Delta_+ = \int_{C_- + C_+} \epsilon \left(1 - \mu^2\right)\,\mathrm{d}\phi. \tag{18b}$$

Note that along $C_\pm$ that $\mathrm{d}\phi$ has sign $\mp$ respectively, thanks to our sign convention. We proceed to integrate:

- Δ_-: Recalling the parameterization for the separatrix $\mu_{sep}(\phi)$ given by Equation 6, we can evaluate explicitly over C_-. This gives result

$$\Delta_- = 2\pi\left(1 - 2\eta\sin I - \eta^2\cos^2 I\right) + 16\cos I\eta^{3/2}\sqrt{\sin I}. \tag{19}$$

- $\Delta_- + \Delta_+$: Note $\mathrm{d}\phi$ changes signs between C_- and C_+. Thus, only terms in Δ_- that also change signs on C_+ contribute to the integral. This allows us to evaluate

$$\Delta_- + \Delta_+ = 32\epsilon\eta^{3/2}\cos I\sqrt{\sin I}. \tag{20}$$

From these two integrals, we obtain

$$P_c = \frac{16\eta^{3/2}\cos I\sqrt{\sin I}}{\pi\left(1 - 2\eta\sin I - \eta^2\cos^2 I\right) + 8\eta^{3/2}\cos I\sqrt{\sin I}}. \tag{21}$$

As evidence, we provide the following table of separatrix capture probabilities in Table 1.

It may be noted that the numerical P_c are systematically low compared to their analytical estimates. This has a clean explanation: initial conditions that start too close to the separatrix violate the assumption where h_i is uniformly distributed on $[-\Delta_-, 0]$. In particular, most of the points near the separatrix and in zone III are escaping points, as can be visually seen in Figure 3. A systematic underdensity of points converging to CS2 (separatrix capture) can be seen on the right hand side of the plot near the separatrix in Figure 4.

A further interesting feature in Figure 4 is a small portion of points in zone II near CS4 at $\phi = 2\pi$ that escape. These points accrue Δ_+ on their first orbit and escape without librating. Visually, this zone is obvious in Figure 3 as the separation between $W_s^{(1)} \cup W_u^{(1)}$ and $W_s^{(0)} \cup W_u^{(0)}$ near $\phi = 2\pi$.

For trajectories originating in zone II, numerical simulations indicate they can never leave the separatrix. This can be understood quantitatively (excepting the few initial conditions in Figure 4 discussed above). For any orbit in zone II that completes a full libration over contour C, the total change in h is given

$$\Delta h = \epsilon \oint_C (1 - \mu^2)\,\mathrm{d}\phi. \tag{22}$$

Since C is a closed contour, any terms that are symmetric on the top and bottom legs of C vanish. If we decompose $\mu(\phi) \equiv \bar{\mu} \pm \mu'(\phi)$ where $\bar{\mu}$ is the average value of $\mu(\phi)$ over C and $\mu'(\phi) \geq 0$

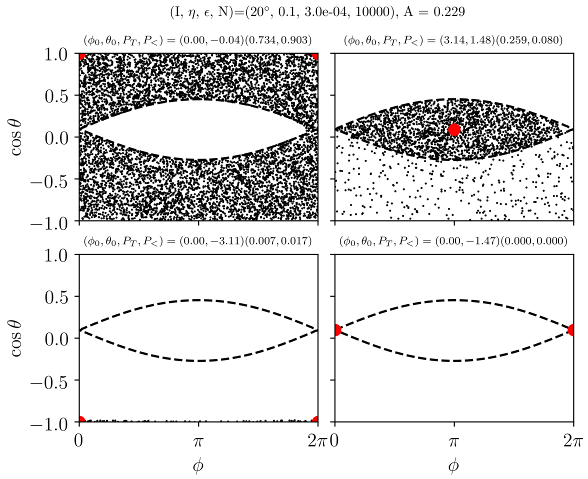

Figure 4. Plot of the CSs that initial conditions converge to. Each subplot has a set of initial conditions (black dots) and the CS (red dot) that each of these initial conditions converge to. Initial conditions are chosen uniformly in (μ, ϕ) coordinates. The parameters for the simulation are in the title.

everywhere, then it is clear

$$\Delta h = 2\epsilon \int_0^{2\pi} 2\bar{\mu}\mu'(\phi)\,\mathrm{d}\phi. \tag{23}$$

Now, since $\mu'(\phi) \geq 0$ everywhere, and $\bar{\mu} \in [\mu_2, \mu_4] > 0$ as well, $\Delta h > 0$ necessarily, and *all full librations in zone II will be driven towards CS2* (the point of maximum h and maximum $H^{(0)}$).

5 PROBLEM 2: ADIABATIC CAPTURE

Here, instead of introducing an aligning perturbation, we will instead adiabatically vary η.

5.1 Spindown Model

We may first consider the unperturbed Hamiltonian system with $\frac{\mathrm{d}\eta}{\mathrm{d}t} = \frac{\eta}{t_\eta}$ growth with characteristic timescale t_η. Again rescaling time $\tau \equiv \alpha t$ and defining $\epsilon \equiv \frac{1}{\alpha t_\eta}$, we obtain

$$\frac{\mathrm{d}\eta}{\mathrm{d}\tau} = \epsilon\eta, \tag{24}$$

where $\epsilon > 0$. Such a model is motivated e.g. when a planet's spin $\hat{s}$ orbits a host star with angular momentum $\hat{l}$ while the star spins down; $\dot{\alpha} < 0$ here, and $\eta' > 0$.

We then seek $\Delta_\pm$, determined by

$$\Delta_\pm = \int_{C_\pm} \frac{\partial h}{\partial \eta}\eta'\,\mathrm{d}\tau, \\ = \int_{C_\pm} \frac{\frac{\partial h}{\partial \eta}}{\phi'}\eta'\,\mathrm{d}\phi. \tag{25}$$

We must proceed carefully since $\phi' \to 0$ at the endpoints of $C_\pm$; careful work shows these zeros cancel against zeros of $\frac{\partial h}{\partial \eta}$, and

$$\Delta_\pm = \int_{C_\pm} \eta'\left(\cos I \mp \sin I\sqrt{\frac{1 - \cos\phi}{2\eta\sin I}}\right)\,\mathrm{d}\phi. \tag{26}$$

η	0.025	0.05	0.1	0.2
Numerical P_c	0.010 ± 0.002	0.029 ± 0.003	0.082 ± 0.004	0.256 ± 0.006
Analytical P_c	0.0112	0.0320	0.0915	0.2627.

Table 1. Capture probability for four different values of η, all using $\epsilon = 3 \times 10^{-4}$. Different values of ϵ were tried $\epsilon \in 10^{[-2,-4]}$ with no effect on P_c. 10000 random initial conditions uniformly distributed in (μ, ϕ) were used for the numerical calculations, of which roughly $1/2$ experience separatrix crossing. Numerical uncertainties are estimated as $\sqrt{N}$ where N is the count per bin.

[t]

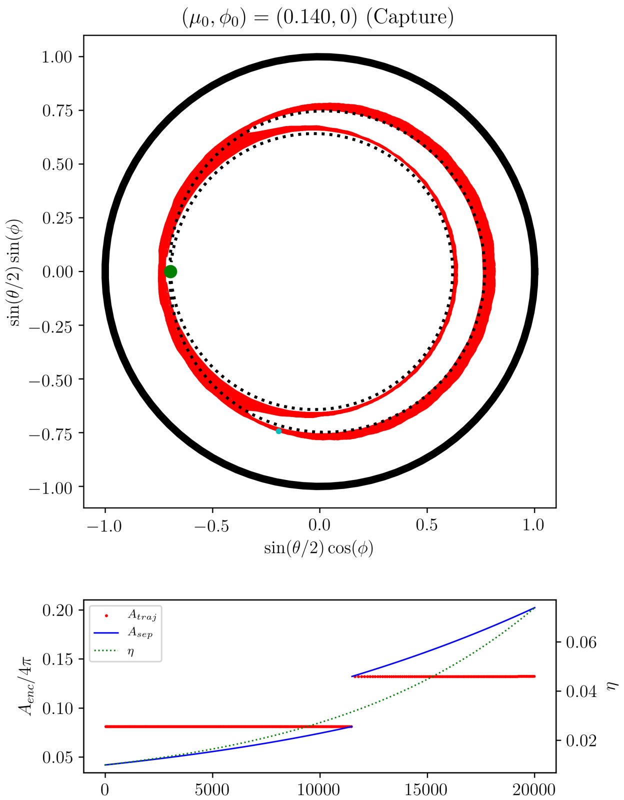

Figure 5. Simulation with initial condition in zone I subject to $\eta' = \epsilon\eta$, where $\epsilon = 10^{-4}$. The top panel shows the trajectory (red) starting with initial condition $\mu_0 = 0.140$, $\phi_0 = 0$ (green dot) and separatrix at separatrix crossing (dashed black) in the labelled coordinates. The end of the simulation is labelled in the blue cyan dot. The bottom panel shows the evolution of the enclosed area by the trajectory (red dots), area of the separatrix (blue) and η (dotted green) over time.

Immediately, we see that if we use $\eta' = \epsilon\eta$, then $\Delta_\pm > 0$ and *all separatrix encounters result in capture* regardless of whether the trajectory originates in zone I or zone III. Since increasing η results in larger separatrix, zone II trajectories will not experience separatrix crossing. Indeed, an example of such a simulation is presented in Figure 5. Further simulations with other initial conditions support the guaranteed capture prediction in this system.

If instead $\epsilon < 0$, then only zone II initial conditions experience separatrix encounter, and since $\Delta_\pm < 0$, all trajectories are ejected as the separatrix shrinks.

5.2 Nontrivial Test Problem

It is clear that η' in Equation 26 being the same sign along both $C_\pm$ is the source of this guaranteed capture. To assess the accuracy of our formalism, we propose instead test problem where η is varied following

$$\eta' = \epsilon\eta\mu. \tag{27}$$

Straightforward evaluation of Equation 26 yields

$$\Delta_\pm = \pm\epsilon\eta_\star \left[2\pi \sin I \pm 12\sqrt{\eta_\star \sin I}\cos I + 2\pi\eta_\star \cos^2 I\right]. \tag{28}$$

It bears noting that we must evaluate these integrals at $\eta = \eta_\star$ the value at separatrix crossing. Since η evolves over time, $\eta_\star$ depends on initial conditions. While one might expect the adiabatic invariance of the action variable determines $\eta_\star$, this turns out to not be the case; we address this in subsection 5.3.

Since $|\Delta_+| > |\Delta_-|$, separatrix encounters originating in zone III always result in capture. However, encounters originating in zone I experience capture probability

$$P_c(\eta_\star) = \frac{24\cos I\sqrt{\eta_\star \sin I}}{2\pi\sin I + 12\sqrt{\eta_\star \sin I}\cos I + 2\pi\eta_\star\cos^2 I}. \tag{29}$$

To test this capture probability, we adopt a slightly different testing methodology than in Section 4. For fixed initial condition (μ_0, ϕ_0) in zone I, we vary the initial $\eta \in [0.01, 0.02]$ and $\epsilon \in 10^{[-3,-2]}$. In this way, every simulation experiences probabilistic separatrix crossing at roughly comparable times. We then repeated this procedure for three different values $I = 10°, 20°, 25°$. A natural spread in $\eta_\star$ was observed at each I value, which permitted comparison to Equation 29 independently. The results for the three I values are presented in Figure 6, where good agreement with Equation 29 is shown.

5.3 Conservation of Adiabatic Invariant

Under the theory of adiabatic invariants (see e.g. Henrard (1982); Landau & Lifshitz (1976)), trajectories following Hamiltonian equations of motion save for small η' conserve action variable I except at separatrix crossing, where

$$I \equiv \frac{1}{2\pi}\oint p\,\mathrm{d}q. \tag{30}$$

I has physical interpretation the enclosed phase space area of trajectories. Its evolution can be seen in Figure 5. Under the assumption I is conserved except at separatrix crossing, $\eta_\star$ is fixed implicitly by $I = A_{sep}(\eta_\star)$ for I the initial value of the action variable. Since A_{sep} is given by Equation 7, it would appear $\eta_\star$ can be predicted exactly.

NOTE: The rest of this section is not very complete.

This turns out to be accurate in subsection 5.1 but not in subsection 5.2, so it's probably non-physical/has to do with $\eta' = 0$ when $\mu = 0$. Not sure whether this is physically useful. Useful formulas for $\frac{\mathrm{d}I}{\mathrm{d}t}$ can be taken from Henrard (1982); Landau & Lifshitz (1976):

$$\frac{\mathrm{d}I}{\mathrm{d}\tau} = \left[\frac{\partial H}{\partial\eta}T(\eta) - \int_0^{T(\eta)} \frac{\partial H}{\partial\eta}\,\mathrm{d}\tau\right]\eta' = -\frac{\partial}{\partial w}\left(\frac{\partial S}{\partial\eta}\right)\eta'. \tag{31}$$

Here, $T(\eta)$ is the period of the orbit, w is the angle variable conjugate to I, and S is the generating function for canonical transformation $\mu = \frac{\partial S}{\partial \phi}, w = \frac{\partial S}{\partial I}$. These expressions are hard to evaluate, but maybe they will tell us how much to expect $\frac{\mathrm{d}I}{\mathrm{d}\tau}$ to deviate from zero near the separatrix?

6 PROBLEM 3: WEAK TIDAL DISSIPATION

6.1 Solution

We consider now the full Cassini State system with under weak tidal friction (see e.g. Lai (2012)). Note that generally $|g|$ is a constant under weak tidal friction, as it is an orbit-orbit coupling term, while $\alpha \propto s$. Defining then s_c critical spin such that $\frac{s}{s_c} \equiv \frac{\alpha}{|g|}$[1] and Ω_1 the spin that $\hat{s}$ is coupled to, we can write down fully coupled evolution equations for (μ, ϕ, s):

$$\frac{\partial \phi}{\partial \tau} = \frac{s}{s_c}\mu - \left(\cos I + \sin I \frac{\mu}{\sqrt{1-\mu^2}}\cos\phi\right), \tag{32a}$$

$$\frac{\partial \mu}{\partial \tau} = -\sin I \sin\phi + \epsilon\left(1-\mu^2\right)\left(\frac{2\Omega_1}{s} - \mu\right), \tag{32b}$$

$$\frac{\mathrm{d}s}{\mathrm{d}\tau} = \epsilon 2\Omega_1\left(\mu - \frac{s}{2\Omega_1}\left(1+\mu^2\right)\right). \tag{32c}$$

The expressions for $H^{(0)}, H_4$ can also be written down

$$H(\mu, \phi; s) = -\frac{s}{s_c}\frac{\mu^2}{2} + \mu\cos I - \sin I\sqrt{1-\mu^2}\cos\phi. \tag{33}$$

$$H_4(s) = -\sin I + \frac{s_c}{2s}\cos^2 I. \tag{34}$$

Note that here s takes the role of adiabatically-varying parameter. Thus, when computing $\Delta_\pm$ along the separatrix using Equation 10, there are two contributions. In particular, we write

$$\Delta_\pm = \int_{C_\pm} \dot{\mu}^{(1)} + \frac{\dot{s}}{\dot{\phi}^{(0)}}\frac{\partial h}{\partial s}\,\mathrm{d}\phi. \tag{35}$$

Both of these integrals were performed in preceeding sections, and we may express in closed form (dropping some terms for simplicity)

$$\Delta_\pm \approx \epsilon\left\{\mp\frac{4\pi\Omega_1}{s} + 8\sqrt{\frac{s_c}{s}}\sin I\right\} + \epsilon\left\{\frac{\Omega_1 s_c}{s^2}\left[\pm 8\sqrt{\frac{s_c}{s}}\sin I\left(\frac{s}{2\Omega_1} - \frac{s_c\cos I}{s}\right) + 4\pi\frac{s_c}{s}\sin I\right]\right\}. \tag{36}$$

We can then compute separatrix capture probability from zone III (which is $P_c = \frac{\Delta_+ + \Delta_-}{\Delta_-}$), again evaluating at $s = s_\star$:

$$P_c(s_\star) = \frac{16\sqrt{\frac{s_c}{s_\star}}\sin I + 8\pi\frac{s_c}{s_\star}\sin I}{\frac{4\pi\Omega_1}{s_\star} - \frac{8\Omega_1 s_c}{s_\star^2}\sqrt{\frac{s_c}{s_\star}}\sin I\left(\frac{s_\star}{2\Omega_1} - \frac{s_c\cos I}{s_\star}\right)}. \tag{37}$$

Note that for $\frac{s_c}{s_\star} < \eta_c$ that no separatrix (or resonance) exists anymore, so we will generally assume $s_\star \gtrsim s_c, \Omega_1$.

To test Equation 37, we generate an evenly spaced grid of initial conditions (μ_0, ϕ_0) and initialize $s_0 = 10$. We then record $s_\star$ and the final ooutcome of the trajectory over many simulations. The agreement of Equation 37 with data can be observed in Figure 7.

[1] s_c has interpretation *critical spin* such that α, $|g|$ are equal.

6.2 Estimating $s_\star$

In Section 5, the capture probability $P_c(\eta_\star)$ depended on $\eta_\star$ which could be determined by conservation of the action varible I. Such an argument is not possible in the weak tidal prescription as the system is dissipitive thanks to $\dot{\mu}^{(1)}$ (see Equation 32).

However, instead we can write down $\frac{\mathrm{d}h}{\mathrm{d}\tau}$, just as Equation 9. Since the initial value of h can be computed from initial conditions, the ODE can simply be integrated numerically to find $\tau_\star$ the separatrix crossing time. In fact, for μ far from the separatrix, $\frac{\mathrm{d}h}{\mathrm{d}\tau} \approx \frac{3s\mu^2}{2s_c}$, predicting

$$\tau_\star = \frac{h(t=0)}{3s\mu^2/2s_c} + C, \tag{38}$$

where C depends on the details of $\frac{\mathrm{d}h}{\mathrm{d}\tau}$ near the separatrix. This is in good agreement with measurement (see top panel of Figure 8).

6.3 High Misalignment as an Attractor

Careful examination of Equation 36 reveals that for sufficiently large s_c, Δ_+ changes sign and becomes positive. When $\Delta_+ < 0$, trajectories in zone I above the separatrix cannot enter the separatrix, as h decreases over an orbit. However, if $\Delta_+ > 0$, then trajectories in zone I can also enter the separatrix. The critical value of s_c where Δ_+ changes sign as a function of s can thus be determined analytically. TODO write down the formula and check it against my numerical solution earlier.

Furthermore, $\frac{\mathrm{d}\mu}{\mathrm{d}\tau} < 0$ for $\mu > \frac{2\Omega_1}{s}$, it is clear that if s is initially large, then aligned states $\mu > 0$ are driven towards misalignment and the separatrix, where they may then be captured for sufficiently large s_c. We find that $s_c \gtrsim 0.5\Omega_1$ is sufficient that an initial spin of $s_0 = 10$ will *always* be captured into CS2. TODO could shore this up a bit, find a good way to plot.

TODO find a clean plot to demonstrate this, I have the data already.

REFERENCES

Guckenheimer J., Holmes P. J., 1983, Nonlinear oscillations, dynamical systems, and bifurcations of vector fields. Springer-Verlag, New York
Henrard J., 1982, Celestial Mechanics and Dynamical Astronomy, 27, 3
Henrard J., Murigande C., 1987, Celestial Mechanics, 40, 345
Lai D., 2012, Monthly Notices of the Royal Astronomical Society, 423, 486
Landau L. D., Lifshitz E. M., 1976, Mechanics. Pergamon press Oxford

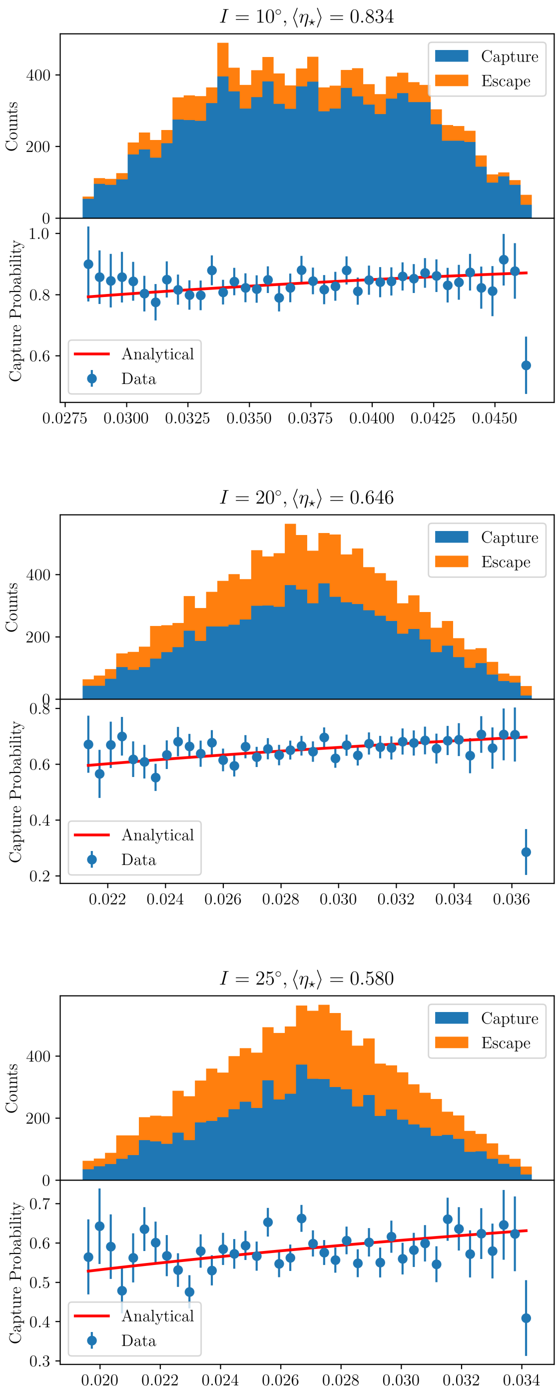

Figure 6. Simulations depicting $P_c(\eta_\star)$ at three different values $I = 10°, 20°, 25°$. The top panel represents the binned outcomes as a function of $\eta_\star$, and the resulting estimates of P_c are compared with the analytical curve (red) from Equation 29 in the bottom panel. Uncertainties in $P_c(\eta_\star)$ from data are estimated as $\sqrt{N}$ where N is the count per bin. Also reported is the average value of $\eta_\star$.

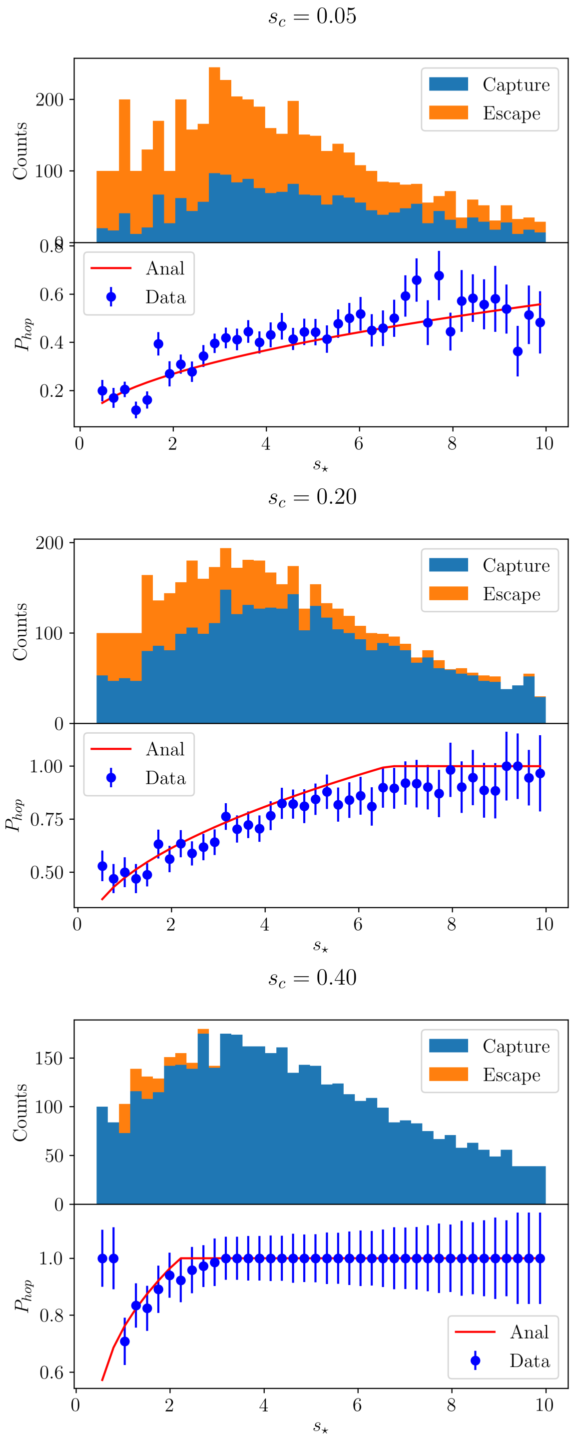

Figure 7. Histogram of simulation and inferred $P_c(s_\star)$ compared with Equation 37. s_c used are numbered at the top of each plot. 10^4 simulations were used for each plot, and a single $I = 20°$ was used.

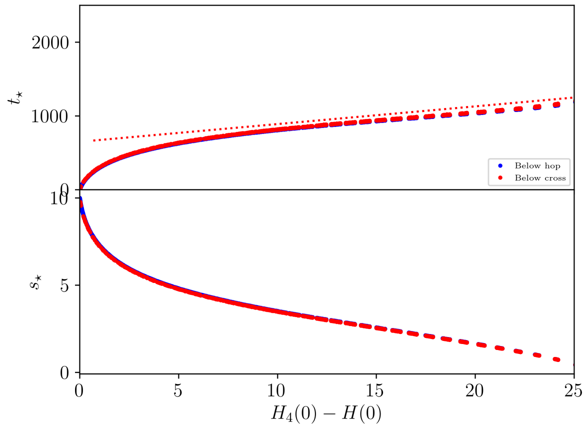

Figure 8. TODO make this plot actually look reasonable. The top and bottom panels show $t_\star, s_\star$ as a function of $-h = H_4 - H$. The dotted red line in the top panel is $t_\star = \frac{h}{3s\mu^2/2s_c} + C$ where C is a fitting parameter determined by the behavior of $\frac{\mathrm{d}h}{\mathrm{d}\tau}$ near the separatrix.